

MAJOR PAPER

Diagnostic Value of DCE-MRI for Differentiating Malignant Adnexal Masses Compared with Contrast-enhanced-T1WI

Satoshi Otani¹, Aki Kido^{1*}, Yuki Himoto¹, Akihiko Sakata¹,
Tomoaki Otani¹, Ryo Kuwahara¹, Yusaku Moribata¹, Naoko Nishio¹,
Ryo Yajima¹, Kyoko Nakao¹, Yasuhisa Kurata¹, Sachiko Minamiguchi²,
Masaki Mandai³, and Yuji Nakamoto¹

Purpose: To compare the diagnostic performance of dynamic contrast-enhanced-MR (DCE-MR) and delayed contrast-enhanced (CE)-MRI added to unenhanced MRI, including diffusion weighted image (DWI) for differentiating malignant adnexal tumors, conducting a retrospective blinded image interpretation study.

Methods: Data of 80 patients suspected of having adnexal tumors by ultrasonography between April 2008 and August 2018 were used for the study. All patients had undergone preoperative MRI and surgical resection at our institution. Four radiologists (two specialized in gynecological radiology and two non-specialized) were enrolled for blinded review of the MR images. A 3-point scale was used: 0 = benign, 1 = indeterminate, and 2 = malignant. Three imaging sets were reviewed: Set A, unenhanced MRI including DWI; Set B, Set A and delayed CE-T1WI; and Set C, Set A and DCE-MRI. Imaging criteria for benign and malignant tumors were given in earlier reports. The diagnostic performance of the three imaging sets of the four readers was calculated. Their areas under the curve (AUCs) were compared using the DeLong method.

Results: Accuracies of Set B were 81%–88%. Those of Set C were 81%–85%. The AUCs of Set B were 0.83 and 0.89. Those of Set C were 0.81–0.86. For two readers, Set A showed lower accuracy and AUC than Set B/Set C (less than 0.80), although those were equivalent in other readers. No significant difference in AUCs was found among the three sequence sets. Intrareader agreement was moderate to almost perfect in Sets A and B, and substantial to almost perfect in Set C.

Conclusion: DCE-MR showed no superiority for differentiating malignant adnexal tumors from benign tumors compared to delayed CE-T1WI with conventional MR and DWI.

Keywords: *dynamic contrast-enhanced magnetic resonance imaging, ovarian tumors, magnetic resonance imaging*

¹Department of Diagnostic Imaging and Nuclear Medicine, Kyoto University Graduate School of Medicine, Kyoto, Kyoto, Japan

²Department of Diagnostic Pathology, Kyoto University Graduate School of Medicine, Kyoto, Kyoto, Japan

³Department of Gynecology and Obstetrics, Kyoto University Graduate School of Medicine, Kyoto, Kyoto, Japan

*Corresponding author: Department of Diagnostic Radiology and Nuclear Medicine, Kyoto University, 57, Shogoin Kawaharacho, Sakyo-ku, Kyoto, Kyoto 606-8507, Japan. Phone: +81-75-751-3760, Fax: +81-75-771-9709, E-mail: akikido@kuhp.kyoto-u.ac.jp



This work is licensed under a Creative Commons Attribution-NonCommercial-NoDerivatives International License.

©2021 Japanese Society for Magnetic Resonance in Medicine

Received: January 5, 2021 | Accepted: July 9, 2021

Introduction

Ovarian tumors, a common disease, are often detected incidentally in women of all ages: about 17% by ultrasonographic (US) surveillance and 4%–5% by CT.^{1,2} Most ovarian tumors are benign, but 10%–15% are malignant tumors.² Among all gynecological cancers, ovarian cancer is the third most frequent gynecologic cancer. It has the worst prognosis mainly because of rapid progression and late onset symptoms.³ Therefore, as a strategy for ovarian tumors, differentiating malignant tumors from benign tumors is important for optimizing treatment and for avoiding inappropriate or inadequate treatment.

US is the primary modality for ovarian tumor evaluation.^{4–6} However, the US accuracy depends on the operator's skill. In fact, the lesions are indeterminate in

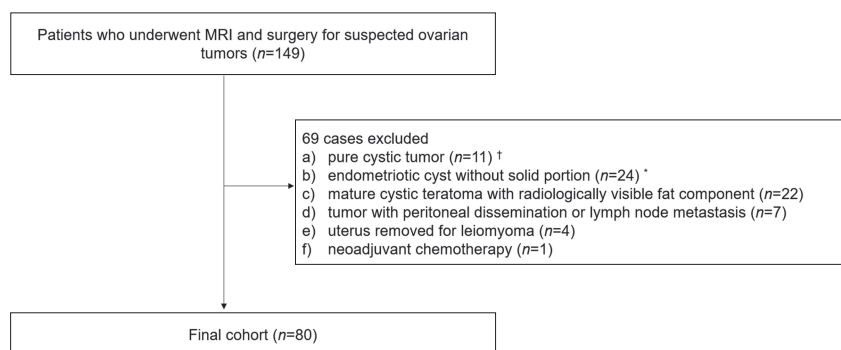


Fig. 1 Flow chart showing patient selection criteria. † Simple cyst without solid lesion. * Completely high signal intensity cyst on fat-suppressed T1-weighted image without mural nodule.

approximately 20% of cases.^{7,8} For additional assessment of those indeterminate ovarian tumors, MRI is useful. Recently, standardization of assessment for ovarian tumors on MRI has been introduced as the ovarian-adnexal reporting and data system (O-RADS).⁹ It has been adopted widely as a prostate imaging reporting and data system (PI-RADS) and breast imaging reporting and data system (BI-RADS).^{10,11} In O-RADS, dynamic contrast-enhanced MR (DCE-MR) and its time–intensity curve (TIC) analysis are recommended in addition to fundamental unenhanced sequences.^{12–14}

Whether DCE-MRI and TIC analysis improve diagnostic performance in the differentiation of adnexal tumor remains controversial. Although several reports have suggested the superiority of DCE-MR to diffusion weighted image (DWI), no report describes a study of comparisons between DCE-MRI and delayed contrast-enhanced T1 weighted image (CE-T1WI).^{13,15} Moreover, DCE-MRI has some shortcomings: longer imaging acquisition time, a certain amount of equipment such as an automatic injector, and more operation for the assessment of dynamic contrast images by creating TIC.

This study was conducted to compare the diagnostic value of DCE-MRI with delayed CE-T1WI in addition to unenhanced MRI with DWI for differentiating malignant adnexal tumors from benign tumors.

Materials and Methods

Patient cohort and lesion characteristics

This retrospective study was approved by the institutional review board of our institution. Informed consent was waived for retrospective analyses. From the institutional database between 2008 April and 2018 August, we included consecutive patients with ipsilateral or bilateral adnexal masses detected by US who underwent preoperative DCE-MRI and surgical resection at our institution. In total, 149 patients met these criteria. Exclusion criteria were set based on an earlier report:¹³ 1) pure cystic tumor (unilocular cyst without solid lesion) ($n = 11$); 2) endometriotic cyst without solid portion (completely high signal intensity [SI] cyst on

fat-suppressed T1WI without mural nodule) ($n = 24$); 3) mature cystic teratoma with radiologically visible fat component ($n = 22$); 4) tumors with peritoneal dissemination or lymph node metastasis suspected on MRI and confirmed histopathologically ($n = 7$); 5) neoadjuvant chemotherapy ($n = 1$); and 6) posthysterectomy ($n = 4$). The final cohort included 80 patients with 92 lesions (Fig. 1). Borderline tumors were classified as malignant lesions. Regarding patient characteristics, the ages of patients were 52.4 ± 15.5 years (mean \pm standard deviation).

MR protocol

All MR studies were performed at our institution using a 3.0-tesla (T) (Trio and Skyra; Siemens Healthineers, Erlangen, Germany) or 1.5-T (Symphony and Avanto; Siemens Healthineers) MRI system with a phased-array body coil. Before each examination, 20 mg of butyl scopolamine (Buscopan; Nippon Boehringer Ingelheim, Tokyo, Japan) was administered by intramuscular injection to reduce bowel motion, unless contraindicated. The MR protocol included axial and sagittal T2 weighted image (T2WI), sagittal T1WI, axial T1WI with fat suppression, axial or sagittal DWI, and axial or sagittal DCE-T1WI. After DCE-T1WI, sagittal and axial CE-T1WI was used with or without fat suppression.

The parameters were as follows: for T2WI, TR/TE 3700–7061/81–108 ms, 200–320 mm FOV, 4–5 mm slice thickness, 150° flip angle (FA), and 250 Hz/pixel bandwidth; for T1WI, TR/TE 400–714/11–13 ms, 200–320 mm FOV, with 4–5 mm slice thickness, 80° FA, and 250 Hz/pixel bandwidth; for DWI, TR/TE 5000–6200/49–58 ms at 3.0 T and 3000–4200/70–76 ms at 1.5 T, FOV 200–320 mm, with 4–5 mm slice thickness, 128 \times 128 matrix size at 3.0 T and 128 \times 90 at 1.5 T, 90° FA, and 1445–2170 Hz/pixel bandwidth. The b-values of DWI were 0, 500, and 1000 s/mm^2 until March 2009 and 0, 100, 500, and 1000 s/mm^2 after July 2009. The apparent diffusion coefficient (ADC) maps were generated automatically using a mono-exponential decay model with all three or four b-values. Fat suppression technique was spectral adiabatic inversion recovery (SPAIR) at 3.0 T and chemical shift selective (CHESS) at 1.5 T.

Table 1 Term criteria for lesion characterization

Sequence	Term	Definition	Reference
DWI + T2WI	Solid component with low SI on T2WI and without high SI on DWI*	SI on T2WI, compared with that of the outer myometrium, SI on DWI, compared with that of urine in the bladder or cerebrospinal fluid	Siegelman et al., ¹⁶ Thomassin-Naggara et al., ¹⁷ Takeuchi et al. ²²
T2WI	Thickened regular septa	Smooth internal wall with thickness ≥ 3 mm within a cyst	Timmerman et al. ¹⁸
	Thickened irregular septa	Localized septal thickening with thickness ≥ 3 mm within a cyst	Timmerman et al., ¹⁸ Levine et al. ²¹
	Vegetations	Solid papillary projections into the cyst cavity from the cyst wall with heights ≥ 3 mm	Timmerman et al., ¹⁸ Hricak et al., ¹⁹ Sohaib. ²⁰
	Solid portion	Suspected of the presence of tissue, including completely solid tumors.	Thomassin-Naggara et al., ¹² Timmerman et al., ¹⁸ Levine et al. ²¹
DWI + T2WI	Solid component with intermediate SI at T2WI and with high SI on DWI*	SI on T2WI, compared with that of the outer myometrium, SI on DWI, compared with that of urine in the bladder or cerebrospinal fluid	Siegelman et al., ¹⁶ Thomassin-Naggara et al., ¹⁷ Takeuchi et al. ²²
DWI + T2WI	Masses with solid components showing high intense papillary architecture with or without low intense internal branching on T2WI	Typical finding of seromucinous borderline tumor	Tanaka et al. ²³
CE-T1WI	Wall enhancement	Enhancement of the wall of cystic lesion	
DCE-MRI	TIC type 1	Slow increase without a well-defined peak	Thomassin-Naggara et al. ^{12,13}
	TIC type 2	Moderate enhancement followed by a plateau	Thomassin-Naggara et al. ^{12,13}
	TIC type 3	More rapid and steeper rise than that of myometrium	Thomassin-Naggara et al. ^{12,13}

DWI was obtained at $b = 1000$ s/mm. CE-T1WI, contrast-enhanced-T1-weighted image; DCE, dynamic contrast-enhanced-MR; DWI, diffusion weighted image; SI, signal intensity; T2WI, T2-weighted image; TIC, time-intensity curve.

After an intravenous bolus injection of 0.2 mmol/kg gadolinium contrast enhancement (Magnevist; Bayer Yakuhin, Osaka, Japan), DCE-T1WI on sagittal or axial planes were obtained. The parameters were TR/TE, 4.696/2.268 ms, 190–260 mm \times 260 mm FOV, 4 mm slice thickness, 10° FA, and 580 Hz/pixel bandwidth. These sequenced images were acquired at 20, 40, 60, 80, 100, 120, and 180 s. Parameters for CE-T1WI (Fast Spin Echo [FSE]) were TR/TE 450–650/9.3–30 ms, 200–320 mm FOV, 4–5 mm slice thickness, 320–512 \times 176–348 matrix size, 90–170° FA, and 125–230 Hz/pixel bandwidth. For CE-T1WI (Gradient Echo [GE]), they were TR/TE 3.2–4.2/1.2–1.5 ms, 260–350 mm FOV, 3–5 mm slice thickness, 320–384 \times 198–230 matrix size, 10–15° FA, and 580 Hz/pixel bandwidth.

MR image analysis

Four radiologists analyzed the MR images. They were two specialized in gynecological imaging (readers 1 and 2: 8 years of experience [RK] and 11 years of experience [YH]) and nonspecialized radiologists in

gynecological imaging (readers 3 and 4: 11 years of experience [AS]; 7 years of experience [TO]). Three imaging sets were prepared for evaluation. Set A included conventional MRI sequences with T1WI, T2WI, T1WI with fat suppression, and DWI with an ADC map. Set B consisted of Set A and delayed CE-T1WI. Set C consisted of Set A and DCE-MRI with TIC. The orders of three imaging sets to review were chosen randomly for respective readers with at least 3 weeks of interval. The readers were informed of the patient ages and were told that the patients were suspected of having adnexal lesions, but they were blinded to US and clinical findings.

Morphological assessment

The readers evaluated the morphological features reported earlier in the literature, as shown in Table 1.^{14,16–23} Before assessment, readers reviewed the definitions and examples of lesion characterization explained by one radiologist (OS) to standardize image interpretation. In all cases, reviewers were

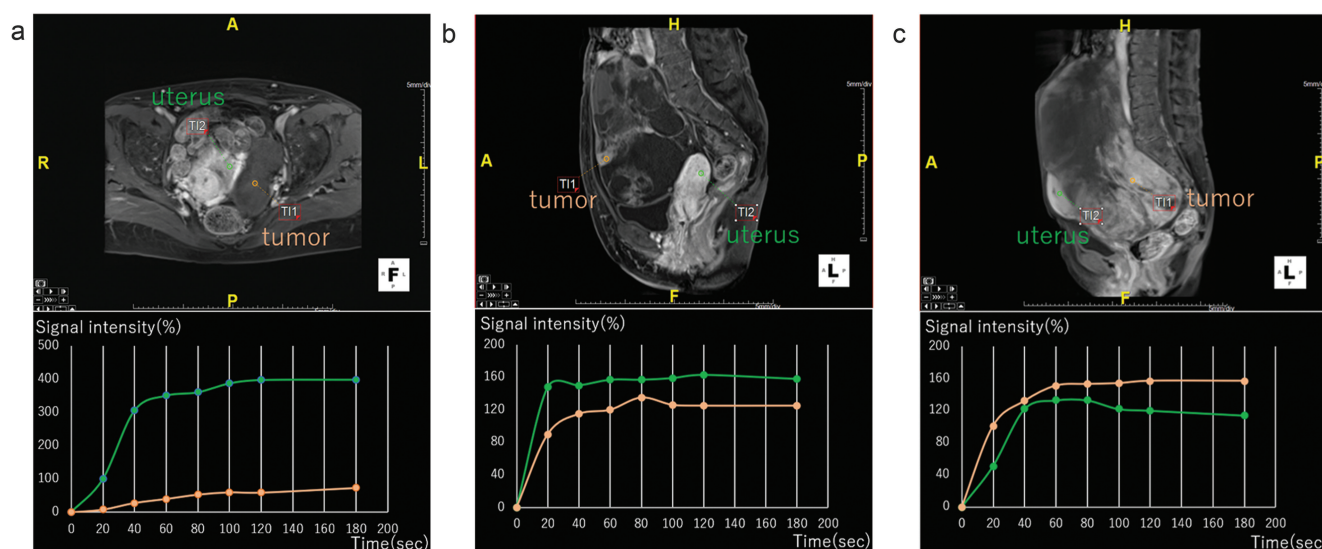


Fig. 2 Analysis of DCE-MRI. Green line, enhanced intensity curve for uterus; orange line, enhanced intensity curve for tumors. (a) Curve type 1: Gradual increase without a well-defined shoulder. (b) Curve type 2: Moderate initial rise relative to that of myometrium followed by a plateau. (c) Curve type 3: Initial rise steeper than that of myometrium. DCE-MRI, dynamic contrast-enhanced MRI.

asked to evaluate the presence or absence of the respective findings. When multiple tumors were found in one patient, each lesion was assessed separately.

Analysis of DCE-MRI

DCE-MRI data were analyzed semi-quantitatively at a workstation (AQ net; TeraRecon, Foster City, CA USA) as described in an earlier report.¹² The TIC was obtained from a circular ROI (> 3 mm diameter) placed manually on the most enhanced solid area of the tumor and on the external myometrium of the uterus by one gynecological radiologist (OS). Four readers classified TICs into three types according to the earlier reports: type 1, a slow increase without a well-defined peak; type 2, a moderate enhancement followed by a plateau; and type 3, a more rapid and steeper rise than that of myometrium¹⁴ (Fig. 2).

Lesion characterization

The imaging criteria of benign tumors were as follows:¹³ 1) solid component with lower SI than the outer myometrium on T2WI and without higher SI than that of urine in the bladder or cerebrospinal fluid on DWI with a b-value of 1000 s/mm²; and 2) a solid component with a type 1 TIC. When these findings were observed, the tumor was considered benign, irrespective of other findings.

Imaging criteria of malignant tumor were as follows: 1) thickened irregular septa, 2) vegetation, 3) solid component with SI higher than or equal to that of the outer myometrium on T2WI and with high SI on DWI with a b-value of 1000 s/mm², 4) a solid component with a type 3 TIC, and 5) masses with solid components

showing high SI papillary architecture with or without low SI internal branching on T2WI. When type 3 TIC was observed, the tumor was considered malignant irrespective of other findings. The other criteria were regarded as suggestive findings.

Based on the imaging criteria presented above, the readers evaluated its malignancy using a 3-point scale: 1, benign; 2, indeterminate; and 3, malignant. When the tumor consisted of only suggestive findings, readers made the final decision comprehensively.

Statistical analysis

To achieve sensitivity, specificity, positive predictive value (PPV), negative predictive value (NPV), and accuracy, 3-point scales of the four readers' evaluations were dichotomized as follows. Scale results of 1 and 2 indicated benign, whereas the scale of 3 indicated malignancy.

Receiver operating characteristic (ROC) curve analyses of 3-point scales of four readers were performed for the respective imaging sets. The area under the curve (AUC) with the standard error using DeLong method was computed. Diagnostic performances of ROC curves were compared using the DeLong method. A *P* value of less than 0.05 was considered to be statistically significant.

Inter-reader agreement was determined using Fleiss' κ , as interpreted by Landis and Koch criteria: a kappa value of 0.81–1.00 represented almost perfect agreement; 0.61–0.80 showed substantial agreement; 0.41–0.60 showed moderate agreement; 0.21–0.40 showed fair agreement; and 0.00–0.20 was indicative of slight agreement.²⁴

All statistical analyses were performed using statistical software (JMP ver. 14; SAS Institute, Cary, NC, USA).

Results

The interval between pretreatment MRI and surgery was 42.6 ± 105.5 days (mean \pm standard deviation). Histopathologic diagnoses are presented in Table 2. Of all cases, 44 were malignant lesions, of which 27 were carcinomas, 13 were borderline tumors, and 4 were other malignant lesions. Of 48 benign cases, 14 were cystadenomas, 10 were fibroma/thecoma/fibrothecoma, 9 were endometriotic lesions, and 15 were various other lesions. Two cases were non-adnexal lesions, suspected as originating from the broad ligament. International Federation of Gynecology and Obstetrics (FIGO) staging of malignant adnexal tumors was as follows: Stage I, $n = 30$; Stage II, $n = 6$; and Stage III, $n = 7$.

Diagnostic performance of three sets of the four readers is presented in Tables 3 and 4. Accuracies of the four readers of three imaging sets were almost identical levels between Set B (81%–88%) and Set C (81%–85%). Even in Set A without CE images, accuracies were almost in identical level with Sets B and C in three of the four readers. Regarding AUC, no significant difference was found between AUCs of any respective imaging sets. Even in Set A of unenhanced MRI, AUC was almost in identical level with Set B or C of other than reader 2. Regarding inter-reader agreement (Table 5), the reader agreement of Set C was better, in fact much better (almost perfect), than either Set A or B.

Table 6 presents cases correctly diagnosed or misdiagnosed solely using Set C. By reader 1's evaluation, one case of ovarian cancer was classified correctly as a malignant tumor. Some benign lesions such as mucinous adenoma (Fig. 3) were diagnosed correctly. Regarding misclassified cases, one case of mucinous borderline tumor and endometrioid carcinoma was misdiagnosed solely by Set C in each of the four readers' evaluations. Benign lesions misclassified by all readers were polycystic ovary (PCO) with torsion.

Discussion

Recently, O-RADS has been recommended for adoption in clinical settings, showing quite high diagnostic values of sensitivity of 93% and specificity of 91%.⁹ Although O-RADS is recommended for use with DCE-MRI and TIC analysis, DCE-MRI has not been adopted adequately for clinical practice because of its longer time necessary for preparation and image interpretation than CE-T1WI. In our study, the addition of DCE-MRI showed no superiority to CE-T1WI or unenhanced MRI with DWI in the differentiation of malignant ovarian tumors from benign tumors. Therefore, our results suggest that a diagnosis can be acquired properly without DCE-MRI.

No significant difference in AUCs was found between CE-T1WI and DCE-MRI by any of the four readers (0.83–0.89 for CE-T1WI and 0.81–0.86 for DCE-MRI). Two readers gave the highest AUC for CE-MRI, whereas one reader gave the highest for DCE-MRI. All readers had more than 5 years

Table 2 Histopathologic diagnoses for all lesions

Histopathological diagnoses	Number
Malignant lesion	44
Carcinoma	
High grade serous carcinoma	8
Clear cell carcinoma	7
Endometrioid adenocarcinoma	8
Mucinous adenocarcinoma	1
Others	3
Borderline tumor	
Mucinous borderline tumor	5
Serous borderline tumor	2
Seromucinous borderline tumor	5
Endometrioid borderline tumor	1
Others	
Granulosa cell tumor	2
Mixed germ cell tumor	1
FATWO*	1
Benign lesion	48
Serous/mucinous cyst adenoma	14
Serous cystadenofibroma	3
Brenner	1
Fibroma/Thecoma/Fibrothecoma	10
Mature cystic teratoma [†]	1
Struma ovarii	2
Endometriotic lesion	9
Hemorrhagic cyst	1
Follicle cyst (PCO)	3
Hemosalpinx	1
SFT*	1
Pelvic inflammatory disease	2

[†] It was difficult to find the component of fat on MR imaging. * They were suspected to originate from the broad ligament. FATWO, female adnexal tumor of probable Wolffian origin; SFT, solitary fibrous tumor; PCO, polycystic ovary.

of clinical experience in radiology. Their long experience suggests that a certain amount of experience enables radiologists to evaluate morphological features adequately and

Table 3 Diagnostic performance of four readers

Reader	1			2			3			4		
	Set A	Set B	Set C	Set A	Set B	Set C	Set A	Set B	Set C	Set A	Set B	Set C
Sensitivity (%)	88	90	93	95	93	88	93	80	86	68	86	90
Specificity (%)	87	85	79	58	72	75	79	90	85	89	77	76
PPV (%)	86	85	80	67	75	76	80	90	84	85	77	75
NPV (%)	89	91	92	93	92	87	92	79	87	75	86	90
Accuracy (%)	88	88	85	76	82	81	85	84	85	79	81	82

Set A: T1WI, T2WI, and DWI. Set B: Set A + delayed CE-T1WI. Set C: Set A + DCE-MRI. Readers 1 and 2 are specialized in gynecological radiology; 3 and 4 are inexpert. CE-T1WI, Contrast-enhanced-T1-weighted image; DCE-MRI, Dynamic contrast-enhanced-MRI; DWI, Diffusion weighed image; NPV, negative predictive value; PPV, positive predictive value; T1WI, T1-weighted image; T2WI, T2-weighted image.

Table 4 List of AUC (95% confidence interval) for four readers

Reader 1	<i>P</i> value [†]	<i>P</i> value*	Reader 2	Reader 3	Reader 4
Set A 0.89 (0.83–0.96)			0.76 (0.69–0.84)	0.86 (0.79–0.93)	0.89 (0.83–0.95)
Set B 0.89 (0.82–0.95)	<i>P</i> = 0.77		0.83 (0.75–0.90)	0.85 (0.78–0.92)	0.83 (0.75–0.91)
Set C 0.86 (0.80–0.93)	<i>P</i> = 0.29	<i>P</i> = 0.29	0.81 (0.73–0.89)	0.86 (0.79–0.93)	0.83 (0.76–0.91)
			<i>P</i> = 0.08	<i>P</i> = 0.74	<i>P</i> = 0.13
			<i>P</i> = 0.21	<i>P</i> = 0.98	<i>P</i> = 0.17
			<i>P</i> = 0.65	<i>P</i> = 0.72	<i>P</i> = 0.9

Set A: T1WI, T2WI, and DWI. Set B: Set A + delayed CE-T1WI. Set C: Set A + DCE-MRI. Readers 1 and 2 are specialized in gynecological radiology; 3 and 4 are inexpert. Data in brackets are 95% confidence intervals. [†] *P* value represents the differences in AUC between Set A and Set B or C. * *P* value represents the differences in AUC between Set B and Set C. AUC, area under the curve; DWI, Diffusion weighed image; CE-T1WI, Contrast-enhanced-T1-weighted image; DCE-MRI, Dynamic contrast-enhanced-MRI; T1WI, T1-weighted image; T2WI, T2-weighted image.

Table 5 Interobserver variation between readers

	Reader 1 and 2	Reader 3 and 4	Reader 1 and 3	Reader 2 and 3	Reader 2 and 4	Reader 1 and 4
Set A	0.58 (0.41–0.75)	0.57 (0.41–0.74)	0.82 (0.71–0.94)	0.66 (0.50–0.81)	0.41 (0.24–0.59)	0.65 (0.49–0.80)
Set B	0.71 (0.57–0.85)	0.58 (0.41–0.75)	0.84 (0.73–0.95)	0.77 (0.65–0.90)	0.53 (0.36–0.71)	0.60 (0.44–0.77)
Set C	0.82 (0.70–0.94)	0.63 (0.47–0.78)	0.82 (0.71–0.94)	0.73 (0.60–0.87)	0.62 (0.46–0.78)	0.75 (0.62–0.89)

Set A: T1WI, T2WI, and DWI. Set B: Set A + delayed CE-T1WI. Set C: Set A + DCE-MRI. Readers 1 and 2 are specialized in gynecological radiology; 3 and 4 are inexpert. Data in brackets are 95% confidence intervals. A kappa value of 0.00–0.20 was indicative of slight agreement, 0.21–0.40 fair agreement, 0.41–0.60 moderate agreement, 0.61–0.80 substantial agreement, and 0.81–1.00 almost perfect agreement. CE-T1WI, Contrast-enhanced-T1-weighted image; DCE-MRI, Dynamic contrast-enhanced-MRI; DWI, Diffusion weighed image; T1WI, T1-weighted image; T2WI, T2-weighted image.

diagnose a patient correctly without employing DCE-MRI. However, the inter-reader agreement between readers was better with Set C. These results suggest that evaluation by TIC is supportive of trainees for differentiation.

To make the most of DCE-MRI, diseases in which only DCE-MRI can diagnose correctly and diseases in which DCE-MRI misdiagnoses should be understood carefully. In our cases, fibromas with quite restricted diffusion and

mucinous adenoma composed of numerous small cysts similar to solid tumors were diagnosed only by Set C, including DCE-MR. Regarding pitfalls of DCE-MRI, PCO with torsion was misdiagnosed by all readers in Set C because of mislocation of ROI. Accordingly, it is noteworthy that there are cases of benign lesions that mimic malignant tumor by noncontrast sequences. It is also notable that misunderstanding of anatomical location might lead to incorrect diagnosis.

Table 6 Cases correctly diagnosed or misdiagnosed only by Set C

	Reader 1	Reader 2	Reader 3	Reader 4
Correctly diagnosed only by Set C	Adenocarcinoma, poorly differentiated, possibly endometrioid carcinoma	Mucinous cystadenoma	Mucinous cystadenoma	Mucinous cystadenoma
		Fibroma	Fibroma	
		Serous cystadenofibroma	Thecoma	
Misdiagnosed only by Set C	PCO with torsion Mucinous cystadenoma Mature cystic teratoma SFT	PCO with torsion	PCO with torsion	PCO with torsion
		Mucinous borderline tumor	Mucinous borderline tumor	
		Mature cystic teratoma	Mature cystic teratoma	Mature cystic teratoma
		SFT	SFT	SFT
		Endometrioid carcinoma		

Set C: T1WI, T2WI, DWI and DCE-MRI. Readers 1 and 2 are specialized in gynecological radiology; 3 and 4 are inexpert. DCE-MRI, Dynamic contrast-enhanced-MRI; DWI, Diffusion weighed image; PCO, polycystic ovary; SFT, solitary fibrous tumor; T1WI, T1-weighted image; T2WI, T2-weighted image.

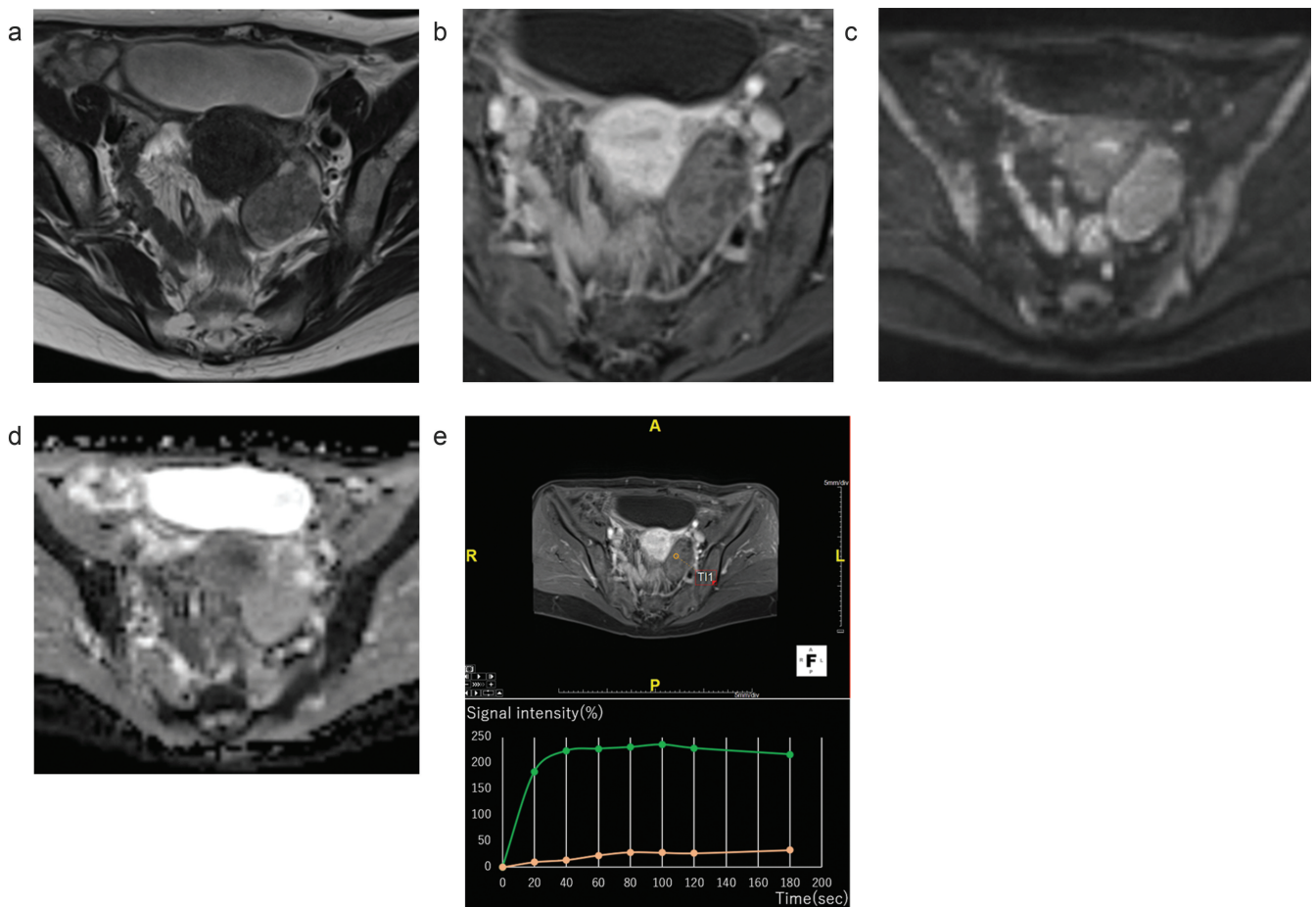


Fig. 3 Case of mucinous cystadenoma, diagnosed correctly only by Set C in three of the four readers. (a) T2-weighted image. (b) Delayed contrast-enhanced T1-weighted image. (c) Diffusion weighted image. (d) Apparent diffusion coefficient. (e) Time-intensity curve (green, uterus; orange, tumor). On T2-weighted image, this tumor appeared a solid tumor, but contrast-enhanced T1-weighted image revealed that it was composed of numerous cysts. Moreover, the time-intensity curve showed type 1 and suggested benignity.

Unenhanced MRI with DWI has comparable diagnostic performance to that of CE-T1WI among all readers. It has been recognized widely that the MRI features that are most predictive of malignancy are an enhanced solid component or vegetation within a cystic lesion and the presence of necrosis within a solid lesion, as well as the presence of ascites and peritoneal deposits.^{19,20,25} Addition of CE-T1WI in the evaluation of adnexal tumor has been well adopted in clinical practice. In fact, DWI, which might reflect tumor cellularity, also contributes to the differentiation of malignant tumors by characterizing solid parts of tumors, especially when contrast administration is contraindicated (i.e. pregnancy or allergy).²⁶ Our results support that unenhanced MRI with DWI is useful instead of CE-T1WI in those cases. Its limitations are also noteworthy, such as vulnerability to motion or susceptibility artifacts related to air, hemorrhages, and metals. The DWI quality is expected to be improved further to omit CE-T1WI.

Our study has some limitations. First, only a small number of patients were included because DCE-MRI is not performed routinely for ovarian tumors and because cases diagnosed reliably using US, such as dermoid cysts and endometriosis cyst, were not included. Second, no resident or fellow radiologist participated in the imaging interpretations in our study. Whether DCE-MRI improves younger radiologists' diagnostic performance or not should be studied further. Third, variations in the MRI scanner occurred because patients were included over an approximately 10-year period. Nonetheless, the diagnostic value of each evaluation set was sufficiently good.

Conclusion

Results show that DCE-MRI has no superiority for differentiating malignant adnexal tumors from benign tumors compared to delayed CE-T1WI. Unenhanced MRI with DWI can be a choice when CE-MRI is contraindicated, considering its comparable diagnostic performance to that of CE-T1WI or DCE-MRI.

Conflicts of Interest

Yuji Nakamoto received honorarium research funding: Shimadzu Corp. Ltd., Eisai Co., Ltd., Nihon Medi-physics Co., Ltd., and FUJIFILM Toyama Chemical Co., Ltd. No other authors have any financial relationship with any organization related to this study.

References

1. Pavlik EJ, Ueland FR, Miller RW, et al. Frequency and disposition of ovarian abnormalities followed with serial transvaginal ultrasonography. *Obstet Gynecol* 2013; 122:210–217.

2. Masch WR, Daye D, Lee SI. MR imaging for incidental adnexal mass characterization. *Magn Reson Imaging Clin N Am* 2017; 25:521–543.
3. Coburn SB, Bray F, Sherman ME, et al. International patterns and trends in ovarian cancer incidence, overall and by histologic subtype. *Int J Cancer* 2017; 140:2451–2460.
4. Geomini P, Kruitwagen R, Bremer GL, et al. The accuracy of risk scores in predicting ovarian malignancy: a systematic review. *Obstet Gynecol* 2009; 113:384–394.
5. Van Gorp T, Veldman J, Van Calster B, et al. Subjective assessment by ultrasound is superior to the risk of malignancy index (RMI) or the risk of ovarian malignancy algorithm (ROMA) in discriminating benign from malignant adnexal masses. *Eur J Cancer* 2012; 48:1649–1656.
6. Maturen KE, Blaty AD, Wasnik AP, et al. Risk stratification of adnexal cysts and cystic masses: clinical performance of society of radiologists in ultrasound guidelines. *Radiology* 2017; 285:650–659.
7. Van Holsbeke C, Daemen A, Yazbek J, et al. Ultrasound experience substantially impacts on diagnostic performance and confidence when adnexal masses are classified using pattern recognition. *Gynecol Obstet Invest* 2010; 69:160–168.
8. Sadowski EA, Paroder V, Patel-Lippmann K, et al. Indeterminate adnexal cysts at US: prevalence and characteristics of ovarian cancer. *Radiology* 2018; 287:1041–1049.
9. Thomassin-Naggara I, Poncelet E, Jalaguier-Coudray A, et al. Ovarian-adnexal reporting data system magnetic resonance imaging (O-RADS MRI) score for risk stratification of sonographically indeterminate adnexal masses. *JAMA Netw Open* 2020; 3:e1919896.
10. Weinreb JC, Barentsz JO, Choyke PL, et al. PI-RADS prostate imaging - reporting and data system: 2015, version 2. *Eur Urol* 2016; 69:16–40.
11. Morris EA, Comstock CE, Lee CH, et al. ACR BI-RADS magnetic resonance imaging. In: *ACR BI-RADS atlas, breast imaging reporting and data system*. Reston: American College of Radiology, 2013.
12. Thomassin-Naggara I, Bazot M, Daraï E, et al. Epithelial ovarian tumors: value of dynamic contrast-enhanced MR imaging and correlation with tumor angiogenesis. *Radiology* 2008; 248:148–159.
13. Thomassin-Naggara I, Toussaint I, Perrot N, et al. Characterization of complex adnexal masses: value of adding perfusion- and diffusion-weighted MR imaging to conventional MR imaging. *Radiology* 2011; 258:793–803.
14. Thomassin-Naggara I, Aubert E, Rockall A, et al. Adnexal masses: development and preliminary validation of an MR imaging scoring system. *Radiology* 2013; 267:432–443.
15. Bernardin L, Dilks P, Liyanage S, et al. Effectiveness of semi-quantitative multiphase dynamic contrast-enhanced MRI as a predictor of malignancy in complex adnexal masses: radiological and pathological correlation. *Eur Radiol* 2012; 22:880–890.
16. Siegelman ES, Outwater EK. Tissue characterization in the female pelvis by means of MR imaging. *Radiology* 1999; 212:5–18.
17. Thomassin-Naggara I, Daraï E, Cuenod CA, et al. Contribution of diffusion-weighted MR imaging for

- predicting benignity of complex adnexal masses. *Eur Radiol* 2009; 19:1544–1552.
18. Timmerman D, Valentin L, Bourne TH, et al. International Ovarian Tumor Analysis (IOTA) Group. Terms, definitions and measurements to describe the sonographic features of adnexal tumors: a consensus opinion from the International Ovarian Tumor Analysis (IOTA) Group. *Ultrasound Obstet Gynecol* 2000; 16:500–505.
 19. Hricak H, Chen M, Coakley FV, et al. Complex adnexal masses: detection and characterization with MR imaging—multivariate analysis. *Radiology* 2000; 214:39–46.
 20. Sohaib SA, Sahdev A, Van Trappen P, et al. Characterization of adnexal mass lesions on MR imaging. *AJR Am J Roentgenol* 2003; 180:1297–1304.
 21. Levine D, Brown DL, Andreotti RF, et al. Society of radiologists in ultrasound. Management of asymptomatic ovarian and other adnexal cysts imaged at US society of radiologists in ultrasound consensus conference statement. *Ultrasound Q* 2010; 26:121–131.
 22. Takeuchi M, Matsuzaki K, Nishitani H. Diffusion-weighted magnetic resonance imaging of ovarian tumors: differentiation of benign and malignant solid components of ovarian masses. *J Comput Assist Tomogr* 2010; 34:173–176.
 23. Tanaka YO, Okada S, Satoh T, et al. Ovarian serous surface papillary borderline tumors form sea anemone-like masses. *J Magn Reson Imaging* 2011; 33:633–640.
 24. Kundel HL, Polansky M. Measurement of observer agreement. *Radiology* 2003; 228:303–308.
 25. Tempany CM, Zou KH, Silverman SG, et al. Staging of advanced ovarian cancer: comparison of imaging modalities—report from the Radiological Diagnostic Oncology Group. *Radiology* 2000; 215:761–767.
 26. Forstner R, Thomassin-Naggara I, Cunha TM, et al. ESUR recommendations for MR imaging of the sonographically indeterminate adnexal mass: an update. *Eur Radiol* 2017; 27:2248–2257.